



HAL
open science

Satellite-observed drop of Arctic sea ice growth in winter 2015-2016

Robert Ricker, Stefan Hendricks, Fanny Girard-Ardhuin, Lars Kaleschke, Camille Lique, Xiangshan Tian-Kunze, Marcel Nicolaus, Thomas Krumpfen

► **To cite this version:**

Robert Ricker, Stefan Hendricks, Fanny Girard-Ardhuin, Lars Kaleschke, Camille Lique, et al.. Satellite-observed drop of Arctic sea ice growth in winter 2015-2016. *Geophysical Research Letters*, 2017, 44, pp.3236-3245. 10.1002/2016GL072244 . insu-03682750

HAL Id: insu-03682750

<https://insu.hal.science/insu-03682750>

Submitted on 1 Jun 2022

HAL is a multi-disciplinary open access archive for the deposit and dissemination of scientific research documents, whether they are published or not. The documents may come from teaching and research institutions in France or abroad, or from public or private research centers.

L'archive ouverte pluridisciplinaire **HAL**, est destinée au dépôt et à la diffusion de documents scientifiques de niveau recherche, publiés ou non, émanant des établissements d'enseignement et de recherche français ou étrangers, des laboratoires publics ou privés.

Copyright

RESEARCH LETTER

10.1002/2016GL072244

Key Points:

- Reduced first-year ice growth linked with anomalous warm winter 2015/2016
- Winter Arctic sea ice extent record low in 2015/2016 associated with a strong drop in thickness
- Volume reduction due to reduced summer multiyear ice replenishment and reduced winter ice growth

Supporting Information:

- Supporting Information S1

Correspondence to:

R. Ricker,
robert.ricker@ifremer.fr

Citation:

Ricker, R., S. Hendricks, F. Girard-Ardhuin, L. Kaleschke, C. Lique, X. Tian-Kunze, M. Nicolaus, and T. Krumpfen (2017), Satellite-observed drop of Arctic sea ice growth in winter 2015–2016, *Geophys. Res. Lett.*, 44, 3236–3245, doi:10.1002/2016GL072244.

Received 7 DEC 2016

Accepted 17 MAR 2017

Accepted article online 21 MAR 2017

Published online 14 APR 2017

Satellite-observed drop of Arctic sea ice growth in winter 2015–2016

Robert Ricker¹ , Stefan Hendricks² , Fanny Girard-Ardhuin¹ , Lars Kaleschke³ ,
Camille Lique¹ , Xiangshan Tian-Kunze³ , Marcel Nicolaus² , and Thomas Krumpfen² 

¹University of Brest, CNRS, IRD, Ifremer, Laboratoire d'Océanographie Physique et Spatiale (LOPS), IUEM, Brest, France, ²Alfred Wegener Institute, Helmholtz Centre for Polar and Marine Research, Bremerhaven, Germany, ³University of Hamburg, Germany

Abstract An anomalous warm winter 2015–2016 lead to the lowest winter ice extent and highlights the sensitivity of the Arctic sea ice. Here we use the 6 year record of an improved sea ice thickness product retrieved from data fusion of CryoSat-2 radar altimetry and Soil Moisture and Ocean Salinity radiometry measurements to examine the impact of recent temperature trend on the Arctic ice mass balance. Between November 2015 and March 2016, we find a consistent drop of cumulative freezing degree days across the Arctic, with a negative peak anomaly of about 1000 degree days in the Barents Sea, coinciding with an Arctic-wide average thinning of 10 cm in March with respect to the 6 year average. In particular, the loss of ice volume is associated with a significant decline of March first-year ice volume by 13%. This reveals that due to the loss of multiyear ice during previous years, the Arctic ice cover becomes more sensitive to climate anomalies.

1. Introduction

A record low in Arctic sea ice maximum winter extent has been observed in 2016, associated with anomalous high winter air temperatures due to an extreme winter Arctic cyclone [Overland and Wang, 2016; Boisvert et al., 2016]. According to the National Center for Environmental Prediction (NCEP) monthly reanalysis near-surface air temperature, the mean temperature at >70°N during November 2015–March 2016 has been at its highest since 1948, reaching –21°C (Figure 1a). The near-surface air temperature is the main controlling factor for thermodynamic growth. Therefore, positive temperature anomalies generally result in lower ice production rates and thinner ice cover in spring. It is the sea ice thickness distribution at the beginning of the melting season that is one of the main drivers for the survivability of sea ice during summer melt. Previous studies have shown that preconditioning by thinner ice cover substantially contributed to the ice extent record minimum in September 2012 [Parkinson and Comiso, 2013]. The observed lengthening of the Arctic melt season leads to reduction of the September ice extent [Stroeve et al., 2014] and prevents the end of summer replenishment of multiyear ice (MYI). This process results in an ongoing loss of MYI [Kwok, 2007] that decreased from about 75% in the mid-1980s to 45% in 2011 [Maslanik et al., 2011] leaving a sea ice cover more sensitive to short-term perturbations [Holland et al., 2006].

Sea ice thickness affects many climate-related processes in the Arctic, such as heat and momentum exchange, freshwater budget, and ocean circulation, as well as marine safety [Nicolaus et al., 2012; Girard-Ardhuin and Ezraty, 2012; Meier et al., 2014; Rabe et al., 2014]. Hence, monitoring the sea ice thickness distributions is essential for our understanding of the ongoing changes of the Arctic sea ice and their consequences. Over the last years, significant progress has been made in retrieving sea ice thickness from satellite observations, especially by laser altimetry from ICESat [Kwok et al., 2009] and radar altimetry from the current European Space Agency mission CryoSat-2 (CS2) [Wingham et al., 2006]. Radar altimetry is used to derive sea ice freeboard that can be transformed into sea ice thickness by assuming hydrostatic equilibrium [Laxon et al., 2003, 2013]. The sensitivity of this method depends on the magnitude of sea ice freeboard; thus, the relative accuracy is generally lower for young and thin ice (thickness <0.8 m) compared to thicker MYI. Sea ice thickness retrievals based on the evaluation of surface emissivity in L band as from the Soil Moisture and Ocean Salinity (SMOS) satellite mission nonetheless can be used to create a sea ice thickness record of thin ice regimes [Kaleschke et al., 2012], where altimetry-based results lack necessary accuracy. With these different data sets, changes in sea

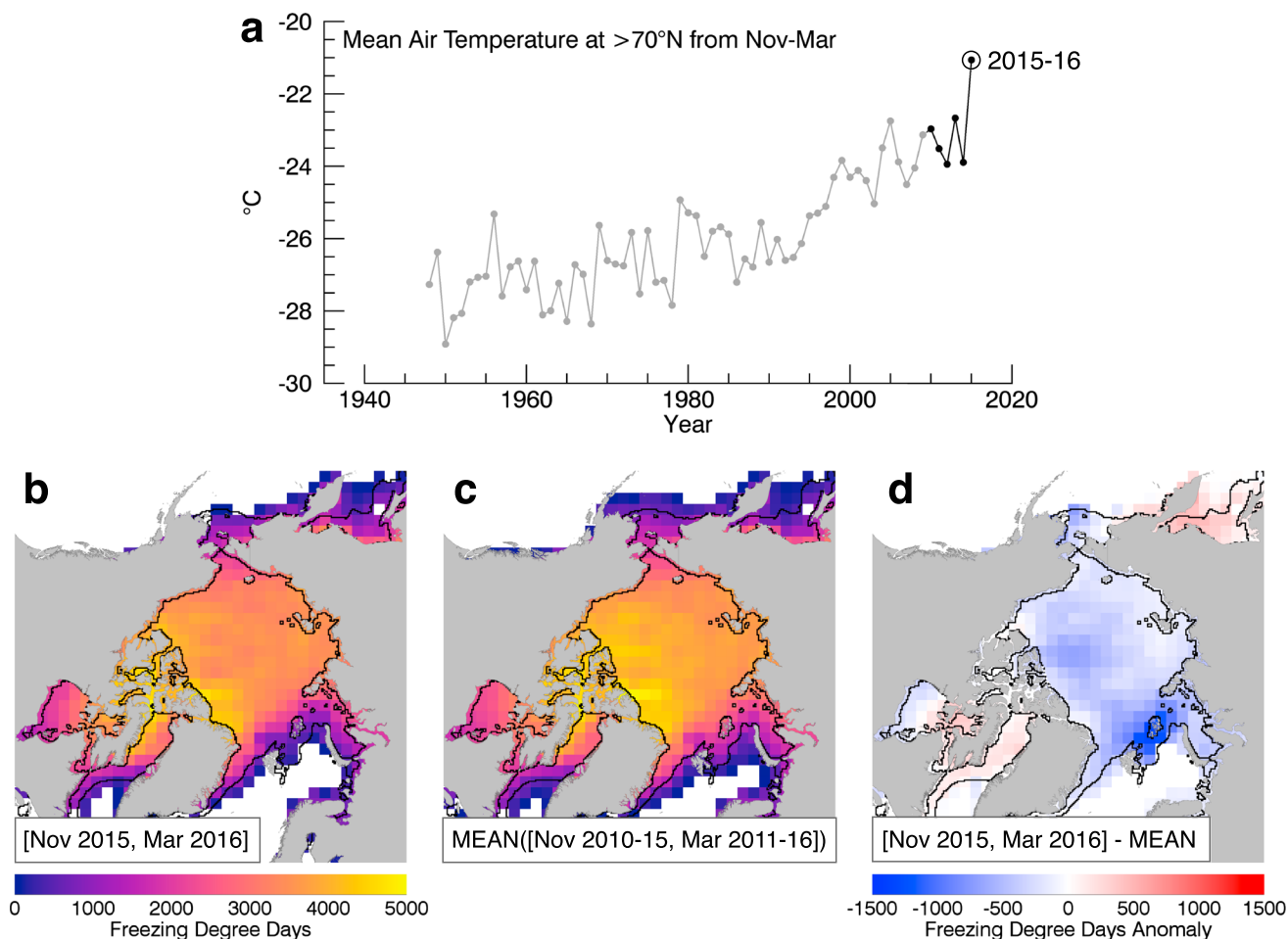


Figure 1. (a) Mean air temperatures above 70°N during November 1948–March 2016, derived from the National Centers for Environmental Prediction (NCEP) monthly reanalysis air temperature, 2 m above surface. (b) Mean Cumulative freezing degree days (FDD) calculated from NCEP air temperature data for November 2015–March 2016. (c) Winter average of FDD for November 2010–March 2011 to November 2015–March 2016. (d) Winter 2015–2016 compared to the winter mean. The black line highlights the mean ice edge during March 2016.

ice thickness can be investigated across the entire sea ice thickness distribution and quantified in the context of the rapid reduction of the Arctic sea ice cover.

After a steady decrease from 2010 to 2012, the first three years of CS2 observations, the Arctic sea ice volume in autumn was substantially larger in 2013 (33%) and 2014 (25%) [Tilling *et al.*, 2015]. Contributing factors were a drop of melting degree days in summer [Tilling *et al.*, 2015] and increased deformation in the Canadian Arctic [Kwok, 2015].

The aim of the present study is to investigate how the Arctic-wide anomalous warm winter temperatures in 2015–2016 affected the thermodynamic ice growth and the sea ice thickness distribution in spring following the positive volume rebound between 2013 and 2015. We use a new merged CS2 and SMOS ice thickness product as well as concentration, displacement, and air temperature anomalies of the previous 6 years to evaluate the state of the sea ice in 2016 and the driving factors of sea ice thickness variability and trends.

2. Data and Methods

2.1. Merged CS2/SMOS Sea Ice Thickness and Volume

An optimal interpolation scheme based on Böhme and Send [2005] and McIntosh [1990] is used to merge CS2 and SMOS ice thickness retrievals. A detailed description of the methodology for combining the CS2 and SMOS data is given by Ricker *et al.* [2017]. Briefly, it allows to merge data sets from diverse sources on a predefined analysis grid, weighted differently based on the uncertainties of the individual products and modeled spatial error covariances. Kaleschke *et al.* [2015] point out the complementary nature of the

relative errors of CS2 and SMOS ice thickness retrievals. While SMOS sensor data show low errors over thin ice (thickness <0.8 m), CS2 relative thickness errors are smaller over thick and increase over thin ice. Relative SMOS uncertainties are about 50% for 0.5 m and 100% for 1 m thick ice. On the other hand, relative CS2 uncertainties are about 40% for 1 m and 20% for 2 m thick ice. This is because of the different methodical approach. SMOS provides brightness temperature observations at L band, which over sea ice are sensitive to the thickness, in particular during the freezeup [Kaleschke et al., 2012]. In contrast, the CS2 radar altimeter can be used to measure the sea ice freeboard, the height of the ice surface above the water level, which can be converted into sea ice thickness assuming hydrostatic equilibrium [Wingham et al., 2006; Laxon et al., 2013; Ricker et al., 2014]. The spatiotemporal coverages of the two products are complementary due to their different orbital inclinations, geometry, sensor type, and footprint sizes. The SMOS retrieval fills significant spatial gaps that are left by CS2 over ice-covered areas in lower latitudes, like Baffin and Hudson Bay. Moreover, the lack of interannual variability in the Warren snow climatology [Warren et al., 1999], which is required for the freeboard-to-thickness conversion, may introduce systematic uncertainties in the CS2 thickness retrieval in the range of 15 cm (MYI)–20 cm (first-year ice; FYI) [Ricker et al., 2014]. The SMOS retrieval, on the other hand, can contribute valuable information, especially in regions with uncertain snow depth estimates. We also note that CS2 thickness retrievals, which alone contribute to the MYI thickness, may be substantially biased in regions with a thick snow cover due to snow volume scattering [Kwok, 2014; Ricker et al., 2015; Armitage and Ridout, 2015]. Both retrievals leave a data gap between mid-April and October due to the limitation of the CS2 and SMOS thickness retrieval algorithms during the melt season [Ricker et al., 2014].

We use weekly means of the Alfred-Wegener-Institute (AWI) CS2 product [Ricker et al., 2014; Hendricks et al., 2016] and the SMOS ice thickness product of the University of Hamburg [Tian-Kunze et al., 2014]. OSI SAF ice concentration [Eastwood, 2012] is applied in order to only allow ice thickness estimates for an ice concentration of >15%. A weight matrix is used to combine the individual products on the analysis grid, yielding weekly sea ice thickness estimates and corresponding error variances of the Northern Hemisphere. The merged weekly thickness retrievals, corresponding to calendar weeks, are projected on a 25 km EASE2 Grid, based on spherical Lambert azimuthal equal-area projection [Brodzik et al., 2012]. Additionally, we compute a weekly mean ice type estimate derived from OSI SAF [Eastwood, 2012] to allow separation between FYI and MYI. The complete data record is provided via the Meereisportal [Grosfeld et al., 2016].

From the merged product, we calculate sea ice volume by multiplying weekly ice concentration (C) with the weekly merged sea ice thickness retrieval (H). We note that H is the average of the ice-covered part of each grid cell. The grid cell volumes are summed up, yielding the total sea ice volume V and the corresponding uncertainty estimate σ_V :

$$V = A \sum_{i=0}^N C_i H_i, \quad \sigma_V = \sum_{i=0}^N V_i \sqrt{\left(\frac{\sigma_{C_i}}{C_i}\right)^2 + \left(\frac{\sigma_{H_i}}{H_i}\right)^2}. \quad (1)$$

The area A of a grid cell equals 625 km². Ice thickness uncertainties σ_{H_i} originate from the merged sea ice thickness product and are represented by the relative error variances scaled with observational variances. Furthermore, we assume an ice concentration uncertainty of $\sigma_{C_i} = 5\%$ to be consistent with Laxon et al. [2013], although we acknowledge that the uncertainty may vary depending on the ice concentration [Ivanova et al., 2014].

2.2. Air Temperature

We use NCEP reanalysis-derived air temperature at 2 m above surface, provided by the National Oceanic and Atmospheric Administration [Kalnay et al., 1996]. The global reanalysis product provides monthly mean temperatures (\bar{T}) with a 2.5° grid resolution. Cumulative freezing degree days (FDD) of a month are calculated using

$$\text{FDD} = n_{\text{md}} \cdot (-1.8^\circ\text{C} - \bar{T}), \quad (2)$$

where n_{md} represents the number of days of a given month. It is important to note that the definition of FDD also considers the magnitude of temperature below the freezing point.

2.3. Ice Drift

Monthly and weekly means of sea ice drift are obtained from the CERSAT/IFREMER database, derived from the merging of the sea ice displacement estimated from daily maps of the Advanced Scatterometer (ASCAT) and

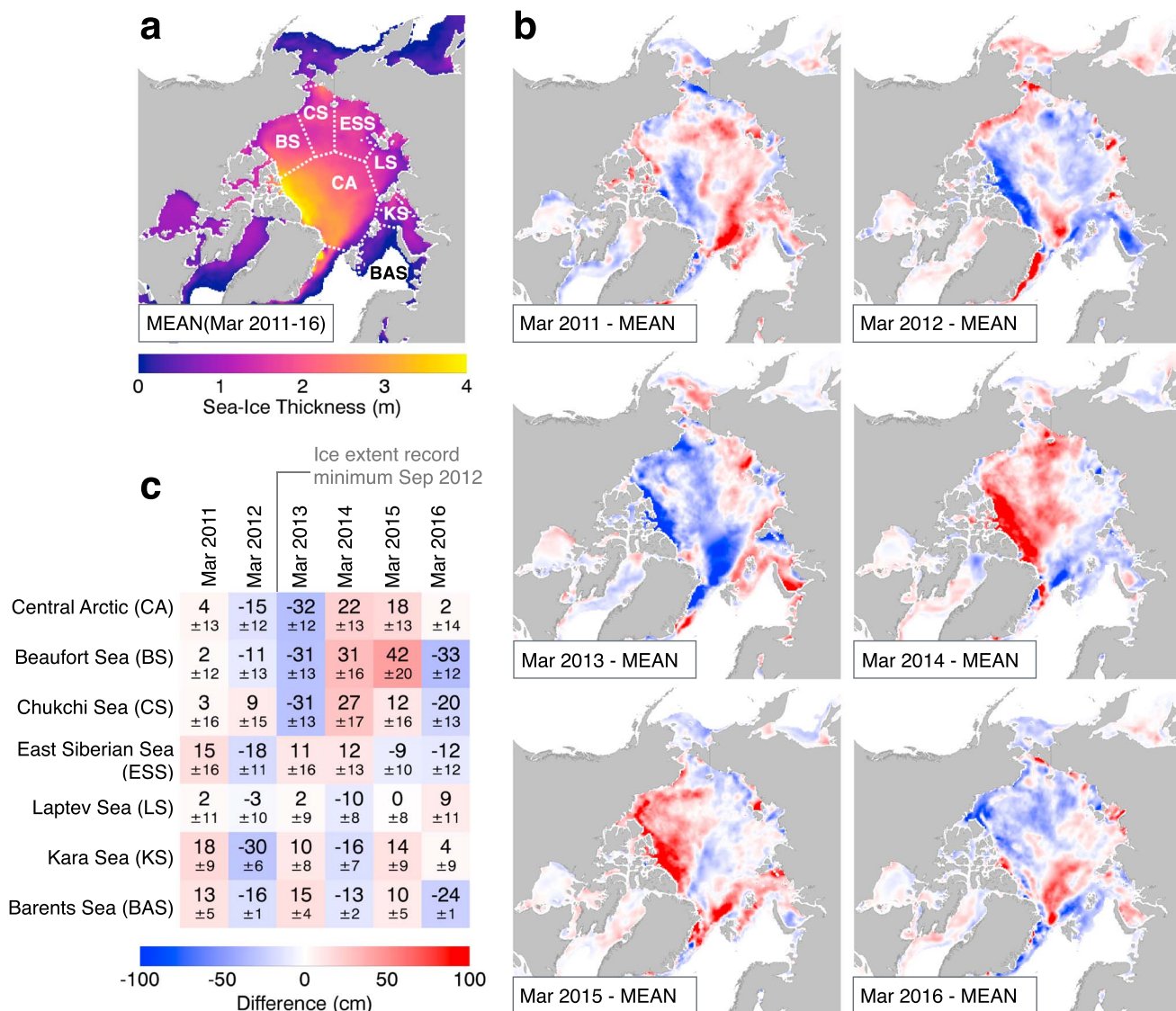


Figure 2. Merged CryoSat-2/SMOS sea ice thickness anomaly for a mean of 3 weeks in March according to the March thickness averaged over 2011–2016: (a) March average over 2011–2016, subdivided into maritime boundaries provided by NSIDC via MAISIE. (b) Yearly March anomalies. (c) Mean anomalies and uncertainties of each year according to the March 2011–2016 mean with respect to the marine domains defined in Figure 2a.

the Special Sensor Microwave Imager (SSM/I) sensors [Girard-Arduin and Ezraty, 2012]. Weekly retrievals of H , C , and ice drift (D) are used to compute the weekly ice volume flux ($F_{x,y}$) in x and y direction:

$$F_{x,y} = gHCD_{x,y}, \tag{3}$$

where $g = 25$ km represents the size of the grid cells. In order to obtain a metric for the sea ice convergence, we compute the volume flux divergence, $\nabla \cdot F$, using a three-point Lagrangian interpolation scheme.

3. Results

In order to obtain a representative thickness distribution for March, we compute the mean of 3 weeks in March for each year. Since the merged product is aligned with calendar weeks, we aim to only include the weeks that are fully in March. Here Figure 2a shows the March average 2011–2016 based on the CS2/SMOS observation period from 2011 to 2016. In order to assess regional variabilities, we divide the Arctic Ocean into domains using the maritime boundaries from the National Snow and Ice Data Center (NSIDC). We then compute the March sea ice thickness anomalies for each region by subtracting the 6 year mean from each March average

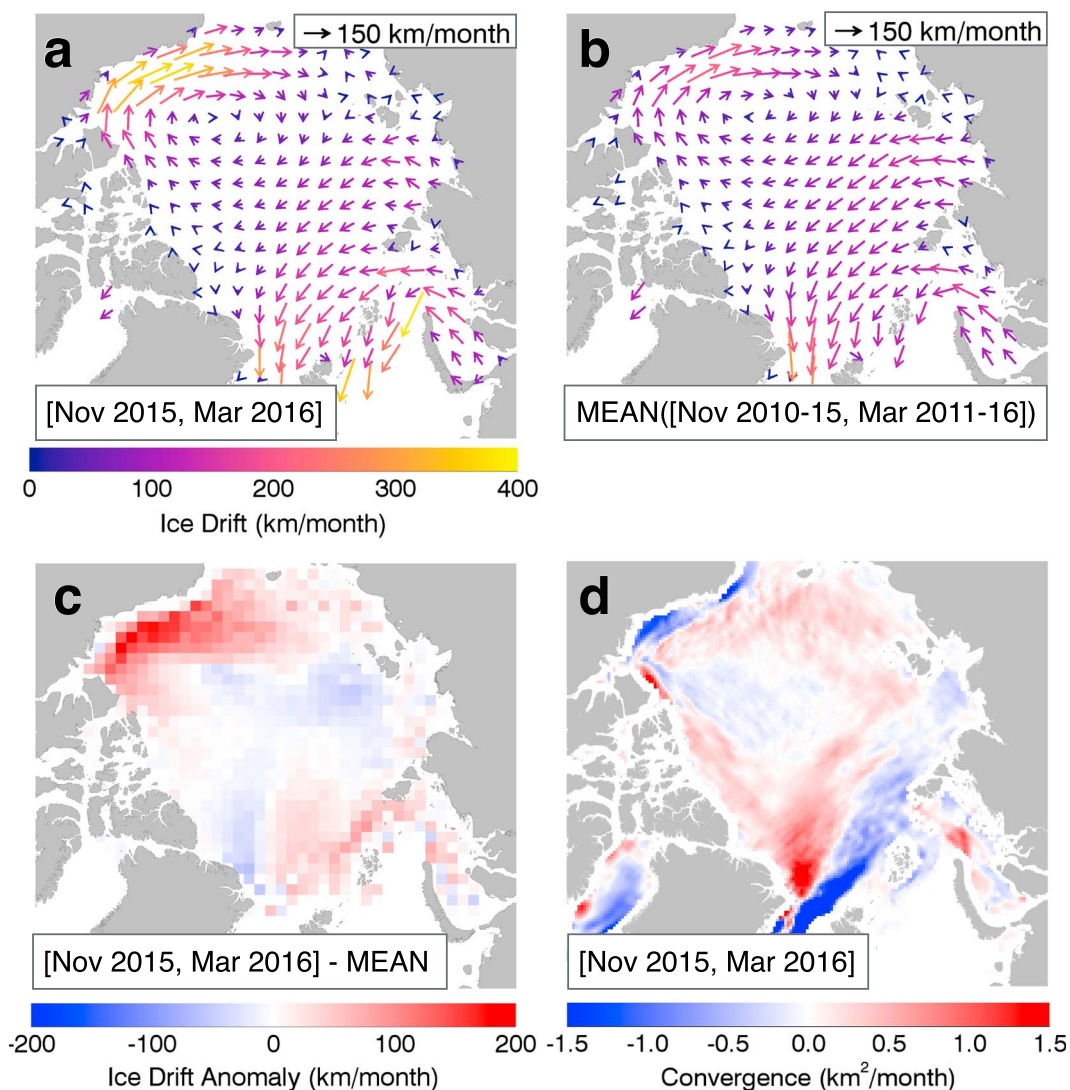


Figure 3. (a) CERSAT/IFREMER sea ice drift, averaged over November 2015–March 2016, and (b) winter ice drift averages for November 2010–March 2011 to November 2015–March 2016. (c) Ice drift magnitude anomaly of November 2015–March 2016. For better visualization in Figures 3a–3c, ice drift data are resampled on a 200 km grid. (d) Ice volume flux convergence of November 2015–March 2016. Positive values indicate convergence, while negative values indicate divergence.

(Figure 2b). Generally, sea ice thickness north of Greenland and Canada during March 2011–2013 is thinner by up to 1 m than the 6 year mean. This is caused by the stark thickness increase in March 2014 of up to 2 m, compared to the previous year, that is setting the mean value. The elevated thickness is maintained until March 2015. In March 2016, we observe a substantial ice thickness drop north of Canada with respect to the March average 2011–2016, effectively erasing the thickness increase of the seasons 2013 and 2014 compared to the first two years of observations. Figure 2c illustrates the thickness anomalies for each region defined in Figure 2a. Beaufort Sea (BS), Chukchi Sea (CS), and the Central Arctic (CA) reveal similar patterns with a negative anomaly of approximately 30 cm in 2013 following the summer extent record minimum in September 2012. The increase of sea ice thickness after the summer of 2013 is mostly observed in the western Arctic and only the BS thickness trend continues to be positive in 2015. The lowest variability is shown by the Laptev Sea (LS), varying between –10 and 9 cm throughout the entire observation record. The strongest change occurs in March 2016 with a decrease of 75 cm in the Beaufort Sea (BS) from the highest anomaly in 2015 (+42 cm) to the lowest in 2016 (–33 cm). Other regions also show noticeably negative anomalies in 2016, such as CS (–21 cm), East Siberian Sea (ESS) (–12 cm), and Barents Sea (BAS) (–24 cm), while other regions (CA, LS, and KS) exhibit negligible positive anomalies.

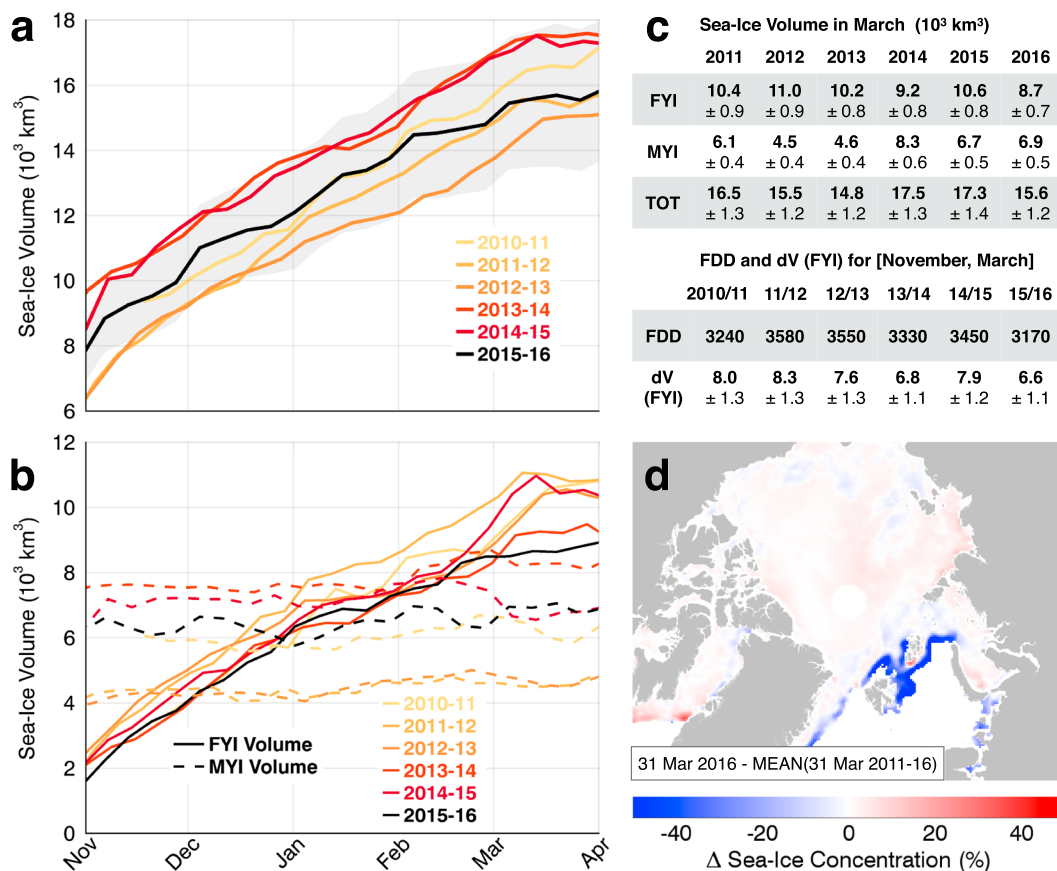


Figure 4. (a) Northern Hemisphere total sea ice volume for 2010–2011 to 2015–2016. Ice volume data stop end of March because ice thickness cannot be retrieved during melting. The grey shadowed area represents the ice volume uncertainty for 2015–2016. (b) First- and multiyear ice (FYI/MYI) volume contributions to the total volume. (c) March ice volume averages and corresponding uncertainties from 2011–2016, as well as spatially averaged FDD over FYI, cumulated from November to March, and corresponding sea ice volume gain (dV). (d) Sea ice concentration anomaly for the 31st of March 2016 with respect to the average of the 6 year record.

To put these changes into the context of thermodynamic forcing, we analyze the NCEP monthly reanalysis air temperature for the winter periods November–March. Figures 1b shows the winter mean cumulative freezing degree days (FDD) for November 2015–March 2016. The mean winter FDD of major parts in the Arctic Basin range between 3000 and 4500, while BAS mean winter FDD reach below 500. Figure 1c shows the cumulative FDD as a 6 year mean for winter (2010–2011 to 2015–2016) and Figure 1d the winter 2015–2016 anomaly. The winter season of 2015–2016 in the central Arctic Basin is generally warmer than 2010–2011 to 2015–2016 mean conditions with anomalies, ranging between -200 and -700 FDD, while the BAS exhibits a negative peak anomaly of about 1000 FDD.

In order to investigate the thickness anomalies in the context of ice dynamics, we assess monthly CERSAT/IFREMER mean ice drift of the same winter period from November to March. Figures 3a and 3b show the 2015–2016 and 2010–2011 to 2015–2016 mean drift, respectively. The anomaly in drift magnitude is presented in Figure 3c, for the drift vectors in Figure 3b. The drift magnitude anomaly is dominated by a strong positive anomaly of up to 200 km/month in the Beaufort Gyre along the Canadian and Alaskan coasts. Increased drift of up to 50 km/month can be observed north of the Fram Strait and minor reduced ice drift north of Siberia and Greenland. The sea ice volume flux convergence of 2015–2016 is shown in Figure 3d. It is characterized by a zone of volume flux convergence north of Greenland of up to $1.5 \text{ km}^2/\text{month}$, with a sharp margin toward an area of strong divergence north of Spitsbergen and toward the Fram Strait. The coastal area in the BS is subject of increased divergence of about $1.5 \text{ km}^2/\text{month}$. The western CA shows a slight divergence of $0.2 \text{ km}^2/\text{month}$. Areas of moderate convergence in the order of $0.4 \text{ km}^2/\text{month}$ are indicated in the CS and ESS.

The overall sea ice conditions are assessed by Arctic-wide sea ice volume in Figure 4. Figure 4a shows the seasonal evolution of total ice volume from November to March. Sea ice volume in November ranges between 6 and $10 \cdot 10^3 \text{ km}^3$ and reaches its maximum in March between 15 and $18 \cdot 10^3 \text{ km}^3$. The increase of sea ice volume is mostly driven by first-year ice growth as seen by separate volume estimates for FYI and MYI (Figure 4b). We find that the MYI volume exhibits almost no seasonal pattern over winter and shows little increase. In agreement with Figure 2, the MYI volume shows decrease from 2010 to 2013 and a rebound in 2013–2014. FYI volume, in contrast, shows substantial larger increase during winter as well as pronounced difference in total volume gain between the years. The average of March 2016 ($8.7 \cdot 10^3 \text{ km}^3$) is the lowest FYI volume of the observation record, coinciding with the lowest FDD (3170) cumulated from November to March and spatially averaged over FYI (Figure 4c). Moreover, the decrease of FYI volume between March 2015 and 2016 is the largest observed drop between the two years ($1.9 \cdot 10^3 \text{ km}^3$). Additionally to the thickness, ice concentration contributes to the ice volume estimate and needs to be considered for interpretation of the 2015–2016 anomalies. The ice concentration anomaly in Figure 4d reveals a reduction in the BAS of about 50% or more at the end of March 2016, compared to the 6 year mean for this day.

4. Discussion

4.1. Sea Ice Thickness and Volume Drop During Winter 2015–2016 in the Context of Interannual Variability

Sea ice thickness shows a substantial spatial and interannual variability. This variability is driven by dynamics and thermodynamics [Zhang *et al.*, 2000; Kwok and Cunningham, 2016] and reaches up to about 30% of the climatological thickness in March. Figure 1 suggests strong coherency in the CA, BS, and CS where thickness decreases from 2011 to 2013 and then substantially increases in 2014. This increase has been discussed in previous works as a result of an anomalous cold summer in 2013 [Tilling *et al.*, 2015] and increased convergence toward the Archipelago, resulting in highly deformed and thicker ice [Kwok, 2015]. The extended observational record shows that elevated thickness levels last until March 2015 and then steeply drop in the following year. This drop is mostly visible in the low FYI volume increase (Figure 4b) over the winter 2015–2016, associated with the anomalous warm air temperatures and a decrease of March MYI thickness north of the Canadian Archipelago (Figure 1b). Here we do not expect a significant impact of the increased winter temperatures, since the thermodynamic growth of snow-covered thick ice ($>2 \text{ m}$) is negligible [Semtner, 1976; Leppäranta, 1993]. However, another driver for the net ice mass loss in March 2016 seems to be a reduced MYI volume in autumn 2015 as the sea ice thickness observation record shows that MYI volume was mostly lower in the winter of 2015–2016, compared to the previous year (Figure 4b). Plausible explanations for the MYI volume reduction are an increase in ice export combined with higher summer melt rates in 2015. Unfortunately, basin-scale summer ice volume estimates are unavailable and ice export estimates through Fram Strait have not been reported after 2014 [Krumpen *et al.*, 2016; Smedsrud *et al.*, 2016]. It is nevertheless clear that above average FYI volume of $10.6 \cdot 10^3 \text{ km}^3$ in March 2015 was not sufficient to replenish MYI to levels of the previous year after the 2015 melt season.

The observed minor trends of MYI volume throughout the winter season combined with distinct offsets between years indicate that processes in summer are the main drivers of MYI volume change. The summer of 2013 with favorable conditions for MYI replenishment creates a buffering effect for MYI thickness with departures from mean conditions that lasts for 2 years or even longer. Nevertheless, in a more seasonal Arctic ice cover, this buffering effect can be countered effectively in individual summers with favorable melting conditions combined with storm events [Zhang *et al.*, 2013], illustrating the enhanced sensitivity to external forcing [Holland *et al.*, 2006]. Currently, it is difficult to assess these processes due to the gap in observational capability of basin-scale summer sea ice thickness.

In FYI-dominated regions, mean thickness in March varies on shorter spatial scales without significant trends. Especially, the LS, KS, and BAS regions show alternating patterns of positive and negative anomalies, while the March LS thickness remains almost invariant. The low variation in LS ice thickness can be explained with the characterizing large extent of undeformed land-fast ice. Its thickness is determined by the thermodynamic ice growth only and therefore exhibits low interannual variability in midwinter [Eicken *et al.*, 2005; Selyuzhenok *et al.*, 2015]. Alternating anomalies in the eastern Arctic are coherent and thus suggest an external forcing. Ice formation in these regions does happen only in winter since the eastern Arctic has mostly been ice-free during the annual minimum of the last years. FYI volume is similar for all years in November, while the following March

volumes show a larger spread. Therefore, besides summer melt, the growth of FYI over the winter season is the second main driver of recent Arctic sea ice volume and its changes.

4.2. Contributing Factors to the Thickness and Volume Anomaly in 2015–2016

Attribution of the processes governing the variability and short-term trends in the Arctic sea ice mass balance is limited by uncertainties and the spatiotemporal resolution in the remote sensing data sets, though first partitions of the thermodynamic and dynamic processes are being investigated [Kwok and Cunningham, 2016].

The positive temperature anomaly coincides with the lowest March FYI volume in 2016 (Figures 1 and 4). We find an average decline of 378 cumulative FDD across the Arctic for 2015–2016 compared to the 6 year mean. The negative peak anomaly in the BAS represents a reduction of FDD by roughly 60% compared to the 6 year average in this region. Applying a simple ice growth model [Anderson, 1961], assuming a constant of proportionality between ice and snow thickness increase of 0.13 and an atmospheric heat transfer coefficient of $45 \text{ W m}^{-2} \text{ K}^{-1}$, we obtain a FYI thickness decrease of 40 cm. This value is larger than the observed FYI thickness reduction (24 cm) in the BAS in 2016 (Figure 1), but roughly comparable. Additionally, the reduction in thickness is accompanied by a decrease in ice concentration of about 50% (Figure 4d), leading to an ice-free area north of Spitsbergen. Our findings in the BAS are in agreement with Boisvert *et al.* [2016], which focuses on the impact of the extreme winter 2015–2016 Arctic cyclone on the Barents and Kara Sea. They found a decrease in sea ice concentration and suggest potential melt of 10 cm in December/January.

Considering the ice motion, we note that a strong Beaufort Gyre drift regime coincides with substantial thinning in the coastal BS in March (Figures 2 and 3). This is probably a positive feedback between drift and thickness, as the drift increase is driven by a combination of wind forcing and a thinner and more mobile ice pack [Spreen *et al.*, 2011; Petty *et al.*, 2016]. We expect that these high drift rates also lead to a faster and more effective transport of MYI from the region north of the Canadian Archipelago into the Chukchi Sea, which may stimulate MYI loss in 2015–2016. However, it seems that as a consequence of the strong Beaufort Gyre, increased ice volume flux divergence contributes to a thinner and thus more vulnerable ice cover. This might result in an early breakup in the BS during the melt season. In contrast, we find an area of thickening north of Greenland and toward the Fram Strait (Figure 2b). Considering the ice drift, Figure 3d suggests that the thicker ice in this area is associated with increased ice volume flux convergence.

The Arctic-wide comparison between FDD over FYI, cumulated in winter, and corresponding FYI volume gain shows correlation between the two parameters (Figure 4c). This linkage suggests that the near-surface air temperature is a driver of FYI volume growth variability in winter. For both parameters, lowest values are shown for 2015–2016 (Figure 4c). However, on regional scale, the linkage between FDD and FYI thickness and volume anomalies can be masked by ice dynamical processes as described above.

In order to separate ice dynamics and thermodynamics, we applied a backtracking approach after Krumpen *et al.* [2016]. We have chosen an endpoint on 30 April at 81.0°N and 37.0°E , located in the northern part of the FDD anomaly that we have observed in March 2016 (Figure S1a). From this point, Lagrangian backtracking is applied to investigate the path of the sea ice during the freezing season. Figure S1b shows the trajectories of the ice floes for each season back to the freezeup in autumn. In 2010–2011, sea ice survived the summer melt. Hence, the starting point is not shown and the trajectory is truncated in September 2010. Figure S1c shows the corresponding sea ice thickness and cumulative FDD along the trajectories. In 2013–2014, when freezeup takes place in September, the FDD value at the end of March exceeds the value found during other seasons when freezeup is delayed. In contrast, in 2015–2016, ice is formed at the end of February, similar to 2011/2012. Hence, we conclude that due to the delay of the freezeup in the BAS, corresponding with a decrease in FDD, sea ice is thinner in spring 2015–2016. This provides evidence that the thickness anomaly in the Barents Sea domain is primarily driven by thermodynamic processes.

The interannual variability of ice mass balance from radar altimetry may be impacted by the currently unknown interannual variability of the snow depth and its potential influence on freeboard retrieval [Ricker *et al.*, 2015; Armitage and Ridout, 2015]. The partially high thickness and volume uncertainties reflect these error sources, and together with the short observation record, they compromise the statistical significance of the thickness and volume anomalies. However, we acknowledge potential incompleteness of the uncertainty estimates. Therefore, the understanding of FYI processes can be improved by merging altimetry-based data sets with complementary observations by L band radiometry. The latter have a higher sensitivity toward

thinner sea ice and thus provide a better observational database of thermodynamic processes that impact the Arctic sea ice mass balance as in the winter of 2015–2016.

5. Conclusion

Sea ice thickness observations from CryoSat-2 and SMOS have shown that sea ice volume in spring 2016 has dropped to levels of 2012, effectively countering a volume gain that started after the summer of 2013 and lasted until spring 2015 in multiyear ice regions. On the one hand, our findings suggest preconditioning by a substantial loss of ice mass during summer 2015, preventing the replenishment of multiyear ice in autumn. On the other hand, anomalous warm air temperatures in the winter season 2015–2016 result in a significant drop of cumulative freezing degree days (FDD) across the Arctic with a negative anomaly of -1000 FDD in the Barents Sea between November 2015 and March 2016. We suggest that this temperature increase leads to reduced ice growth and therefore to a generally thinner ice cover in March compared to the 6 year mean, preconditioning the record low of Arctic sea ice maximum winter extent. At the same time, our results highlight the importance of winter sea ice growth as a key component for sea ice mass balance studies and to assess changes and variability of the Arctic ice cover. Compared to the 6 year average, we find a mean ice thickness decrease of 10 cm in March 2016 across the Arctic, with maxima of 33 cm in the Beaufort Sea and 24 cm in the Barents Sea. These regional thickness anomalies result from an interplay between ice dynamics and thermodynamics. While the Barents Sea thinning seems to be a result of a temperature increase, thickness reduction in the Beaufort Sea seems to be associated to ice volume flux divergence. This is due to an ice drift anomaly of up to $+200$ km/month in the Beaufort Gyre, favoring early breakup in the Beaufort Sea. Nevertheless, an Arctic-wide assessment of winter FDD and corresponding first-year ice volume gain indicates a linkage between near-surface winter air temperature and spring first-year ice volume, revealing the lowest values for both parameters in 2015–2016. Our study points out that the Arctic ice cover is getting more and more sensitive to climate anomalies as first-year ice replaces multiyear ice, which shows little change over the winter seasons, whereas first-year ice is more sensitive to changes in the thermodynamic forcing during winter. However, future work with coupled dynamic-thermodynamic sea ice models is needed to be able to quantitatively separate the effect of dynamic and thermodynamic processes.

Acknowledgments

This work has been conducted in the framework of the European Space Agency project SMOS+ Sea Ice (contracts 4000101476/10/NL/CT and 4000112022/14/I-AM) and the project: Spaceborne observations for detecting and forecasting sea ice cover extremes (SPICES) funded by the European Union (H2020) (Grant: 640161). Moreover, this study is associated with the Deutsche Forschungsgemeinschaft (DFG EXC177) and the German Federal Ministry of Economics and Technology (Grant 50EE1008). CryoSat-2/SMOS data from 2010–2016 are provided by <http://www.meereisportal.de> (Grant REKLIM-2013-04).

References

- Anderson, D. L. (1961), Growth rate of sea ice, *J. Glaciol.*, *3*(30), 1170–1172.
- Armitage, T. W. K., and A. L. Ridout (2015), Arctic sea ice freeboard from altika and comparison with cryosat-2 and operation icebridge, *Geophys. Res. Lett.*, *42*, 6724–6731, doi:10.1002/2015GL064823.
- Böhme, L., and U. Send (2005), Objective analyses of hydrographic data for referencing profiling float salinities in highly variable environments, *Deep Sea Res.*, *52*(3), 651–664.
- Boisvert, L. N., A. A. Petty, and J. C. Stroeve (2016), The impact of the extreme winter 2015/16 arctic cyclone on the barents–kara seas, *Mon. Weather Rev.*, *144*(11), 4279–4287, doi:10.1175/MWR-D-16-0234.1.
- Brodzik, M. J., B. Billingsley, T. Haran, B. Raup, and M. H. Savoie (2012), Ease-grid 2.0: Incremental but significant improvements for earth-gridded data sets, *ISPRS Int. J. Geo Info.*, *1*(1), 32–45, doi:10.3390/ijgi1010032.
- Eastwood, S. (2012), *OSI SAF Sea Ice Product Manual*, v3.8 ed., MetNo, Norway.
- Eicken, H., I. Dmitrenko, K. Tyshko, A. Darovskikh, W. Dierking, U. Blahak, J. Groves, and H. Kassens (2005), Zonation of the laptev sea landfast ice cover and its importance in a frozen estuary, *Global Planet. Change*, *48*(1–3), 55–83, doi:10.1016/j.gloplacha.2004.12.005, arctic Siberian Shelf Environments.
- Girard-Ardhuin, F., and R. Ezraty (2012), Enhanced arctic sea ice drift estimation merging radiometer and scatterometer data, *IEEE Trans. Geosci. Remote Sens.*, *50*(7), 2639–2648, doi:10.1109/TGRS.2012.2184124.
- Grosfeld, K., et al. (2016), Online sea-ice knowledge and data platform, in *Alfred Wegener Institute for Polar and Marine Research and German Society of Polar Research*, vol. 85, pp. 143–155, Polarforschung, Bremerhaven, Germany, doi:10.2312/polfor.2016.011.
- Hendricks, S., R. Ricker, and V. Helm (2016), User Guide – AWI CryoSat-2 Sea Ice Thickness Data Product (v1.2), AWI, Germany. [Available at <http://epic.awi.de/41242/>]
- Holland, M. M., C. M. Bitz, and B. Tremblay (2006), Future abrupt reductions in the summer arctic sea ice, *Geophys. Res. Lett.*, *33*, L23503, doi:10.1029/2006GL028024.
- Ivanova, N., O. M. Johannessen, L. T. Pedersen, and R. T. Tonboe (2014), Retrieval of arctic sea ice parameters by satellite passive microwave sensors: A comparison of eleven sea ice concentration algorithms, *IEEE Trans. Geosci. Remote Sens.*, *52*(11), 7233–7246, doi:10.1109/TGRS.2014.2310136.
- Kaleschke, L., X. Tian-Kunze, N. Maaß, M. Mäkynen, and M. Drusch (2012), Sea ice thickness retrieval from smos brightness temperatures during the arctic freeze-up period, *Geophys. Res. Lett.*, *39*, L05501, doi:10.1029/2012GL050916.
- Kaleschke, L., X. Tian-Kunze, N. Maas, R. Ricker, S. Hendricks, and M. Drusch (2015), Improved retrieval of sea ice thickness from smos and cryosat-2, in *IEEE International on Geoscience and Remote Sensing Symposium (IGARSS), IEEE Conference Proceedings*, pp. 5232–5235, Milan, Italy, 26–31 July.
- Kalnay, E., et al. (1996), The ncep/ncar 40-year reanalysis project, *Bull. Am. Meteorol. Soc.*, *77*(3), 437–471.
- Krumpen, T., R. Gerdes, C. Haas, S. Hendricks, A. Herber, V. Selyuzhenok, L. Smedsrud, and G. Spreen (2016), Recent summer sea ice thickness surveys in fram strait and associated ice volume fluxes, *Cryosphere*, *10*(2), 523–534, doi:10.5194/tc-10-523-2016.
- Kwok, R. (2007), Near zero replenishment of the arctic multiyear sea ice cover at the end of 2005 summer, *Geophys. Res. Lett.*, *34*, L05501, doi:10.1029/2006GL028737.

- Kwok, R. (2014), Simulated effects of a snow layer on retrieval of cryosat-2 sea ice freeboard, *Geophys. Res. Lett.*, *41*, 5014–5020, doi:10.1002/2014GL060993.
- Kwok, R. (2015), Sea ice convergence along the arctic coasts of greenland and the canadian arctic archipelago: Variability and extremes (1992–2014), *Geophys. Res. Lett.*, *42*, 7598–7605, doi:10.1002/2015GL065462.
- Kwok, R., and G. F. Cunningham (2016), Contributions of growth and deformation to monthly variability in sea ice thickness north of the coasts of greenland and the canadian arctic archipelago, *Geophys. Res. Lett.*, *43*, 8097–8105, doi:10.1002/2016GL069333.
- Kwok, R., G. F. Cunningham, M. Wensnahan, I. Rigor, H. J. Zwally, and D. Yi (2009), Thinning and volume loss of the arctic ocean sea ice cover: 2003–2008, *J. Geophys. Res.*, *114*, C07005, doi:10.1029/2009JC005312.
- Laxon, S., N. Peacock, and D. Smith (2003), High interannual variability of sea ice thickness in the arctic region, *Nature*, *425*(6961), 947–950.
- Laxon, S. W., et al. (2013), Cryosat-2 estimates of arctic sea ice thickness and volume, *Geophys. Res. Lett.*, *40*, 732–737, doi:10.1002/grl.50193.
- Leppäranta, M. (1993), A review of analytical models of sea-ice growth, *Atmos. Ocean*, *31*(1), 123–138.
- Maslanik, J., J. Stroeve, C. Fowler, and W. Emery (2011), Distribution and trends in arctic sea ice age through spring 2011, *Geophys. Res. Lett.*, *38*, L13502, doi:10.1029/2011GL047735.
- McIntosh, P. C. (1990), Oceanographic data interpolation: Objective analysis and splines, *J. Geophys. Res.*, *95*(C8), 13,529–13,541.
- Meier, W. N., et al. (2014), Arctic sea ice in transformation: A review of recent observed changes and impacts on biology and human activity, *Rev. Geophys.*, *52*, 185–217, doi:10.1002/2013RG000431.
- Nicolaus, M., C. Katlein, J. Maslanik, and S. Hendricks (2012), Changes in arctic sea ice result in increasing light transmittance and absorption, *Geophys. Res. Lett.*, *39*, L24501, doi:10.1029/2012GL053738.
- Overland, J. E., and M. Wang (2016), Recent extreme arctic temperatures are due to a split polar vortex, *J. Clim.*, *29*(15), 5609–5616, doi:10.1175/JCLI-D-16-0320.1.
- Parkinson, C. L., and J. C. Comiso (2013), On the 2012 record low arctic sea ice cover: Combined impact of preconditioning and an august storm, *Geophys. Res. Lett.*, *40*, 1356–1361, doi:10.1002/grl.50349.
- Petty, A. A., J. K. Hutchings, J. A. Richter-Menge, and M. A. Tschudi (2016), Sea ice circulation around the beaufort gyre: The changing role of wind forcing and the sea ice state, *J. Geophys. Res. Oceans*, *121*, 3278–3296, doi:10.1002/2015JC010903.
- Rabe, B., M. Karcher, F. Kauker, U. Schauer, J. M. Toole, R. A. Krishfield, S. Pisarev, T. Kikuchi, and J. Su (2014), Arctic ocean basin liquid freshwater storage trend 1992–2012, *Geophys. Res. Lett.*, *41*, 961–968, doi:10.1002/2013GL058121.
- Ricker, R., S. Hendricks, V. Helm, H. Skourup, and M. Davidson (2014), Sensitivity of CryoSat-2 Arctic sea-ice freeboard and thickness on radar-waveform interpretation, *Cryosphere*, *8*(4), 1607–1622, doi:10.5194/tc-8-1607-2014.
- Ricker, R., S. Hendricks, D. K. Perovich, V. Helm, and R. Gerdes (2015), Impact of snow accumulation on cryosat-2 range retrievals over arctic sea ice: An observational approach with buoy data, *Geophys. Res. Lett.*, *42*, 4447–4455, doi:10.1002/2015GL064081.
- Ricker, R., S. Hendricks, L. Kaleschke, X. Tian-Kunze, J. King, and C. Haas (2017), A weekly arctic sea-ice thickness data record from merged cryosat-2 and smos satellite data, *Cryosphere Discuss.*, *2017*, 1–27, doi:10.5194/tc-2017-4.
- Selyuzhenok, V., T. Krumpfen, A. Mahoney, M. Janout, and R. Gerdes (2015), Seasonal and interannual variability of fast ice extent in the southeastern laptev sea between 1999 and 2013, *J. Geophys. Res. Oceans*, *120*, 7791–7806, doi:10.1002/2015JC011135.
- Semtner, A. J. (1976), A model for the thermodynamic growth of sea ice in numerical investigations of climate, *J. Phys. Oceanogr.*, *6*(3), 379–389.
- Smedsrud, L. H., M. H. Halvorsen, J. C. Stroeve, R. Zhang, and K. Kloster (2016), Fram strait sea ice export variability and september arctic sea ice extent over the last 80 years, *Cryosphere Discuss.*, *2016*, 1–29, doi:10.5194/tc-2016-79.
- Spreen, G., R. Kwok, and D. Menemenlis (2011), Trends in arctic sea ice drift and role of wind forcing: 1992–2009, *Geophys. Res. Lett.*, *38*, L19501, doi:10.1029/2011GL048970.
- Stroeve, J. C., T. Markus, L. Boisvert, J. Miller, and A. Barrett (2014), Changes in arctic melt season and implications for sea ice loss, *Geophys. Res. Lett.*, *41*, 1216–1225, doi:10.1002/2013GL058951.
- Tian-Kunze, X., L. Kaleschke, N. Maaß, M. Mäkynen, N. Serra, M. Drusch, and T. Krumpfen (2014), Smos-derived thin sea ice thickness: algorithm baseline, product specifications and initial verification, *Cryosphere*, *8*(3), 997–1018, doi:10.5194/tc-8-997-2014.
- Tilling, R. L., A. Ridout, A. Shepherd, and D. J. Wingham (2015), Increased arctic sea ice volume after anomalously low melting in 2013, *Nat. Geosci.*, *8*(8), 643–646.
- Warren, S. G., I. G. Rigor, N. Untersteiner, V. F. Radionov, N. N. Bryazgin, Y. I. Aleksandrov, and R. Colony (1999), Snow depth on arctic sea ice, *J. Clim.*, *12*(6), 1814–1829.
- Wingham, D., et al. (2006), Cryosat: A mission to determine the fluctuations in earth's land and marine ice fields, *Adv. Space Res.*, *37*(4), 841–871, doi:10.1016/j.asr.2005.07.027.
- Zhang, J., D. Rothrock, and M. Steele (2000), Recent changes in arctic sea ice: The interplay between ice dynamics and thermodynamics, *J. Clim.*, *13*(17), 3099–3114, doi:10.1175/1520-0442(2000)013<3099:RCIASI>2.0.CO;2.
- Zhang, J., R. Lindsay, A. Schweiger, and M. Steele (2013), The impact of an intense summer cyclone on 2012 arctic sea ice retreat, *Geophys. Res. Lett.*, *40*, 720–726, doi:10.1002/grl.50190.